Smoke control in tunnel with a transverse ventilation system: An experimental study

Fateh Chaabat, Pietro Salizzoni, Mathieu Creyssels, Antoine Mos, Joy Wingrave, Horacio Correia, Massimo Marro

▶ **To cite this version:**

Fateh Chaabat, Pietro Salizzoni, Mathieu Creyssels, Antoine Mos, Joy Wingrave, et al.. Smoke control in tunnel with a transverse ventilation system: An experimental study. Building and Environment, 2020, 167, pp.106480. 10.1016/j.buildenv.2019.106480 . hal-03234698

HAL Id: hal-03234698
https://hal.science/hal-03234698

Submitted on 20 Jul 2022

HAL is a multi-disciplinary open access archive for the deposit and dissemination of scientific research documents, whether they are published or not. The documents may come from teaching and research institutions in France or abroad, or from public or private research centers.

L'archive ouverte pluridisciplinaire **HAL**, est destinée au dépôt et à la diffusion de documents scientifiques de niveau recherche, publiés ou non, émanant des établissements d'enseignement et de recherche français ou étrangers, des laboratoires publics ou privés.

Distributed under a Creative Commons Attribution - NonCommercial 4.0 International License

Version of Record: https://www.sciencedirect.com/science/article/pii/S0360132319306924
Manuscript_864c953e736ea407aaa749db8d04df69

Smoke control in tunnel with a transverse ventilation system: an experimental study

Chaabat[1], F., Salizzoni[1], P., Creyssels[1], M., Mos[2], A., Wingrave[3], J., Correia[1], H., Marro[1], M.,

[1]*Laboratoire de Mécanique des Fluides et d'Acoustique, University of Lyon, CNRS UMR 5509 Ecole Centrale de Lyon, INSA Lyon, Université Claude Bernard, 36, avenue Guy de Collongue, 69134 Ecully, France*

[2]*Centre d'Etudes des Tunnels, avenue François Mitterrand, 69500 Bron, France*

[3]*University of Surrey, Guildford, Surrey, United Kingdom*

ABSTRACT

We carried out a series of experiments in a small-scale tunnel to study the confinement of smoke flow between two exhaust vents located on either side of a buoyant source placed at ground level within a ventilated tunnel. The objective of our study is to quantify the influence of the shape and the position (with respect to the tunnel axis) of the dampers, including the specific case of full-width dampers, on the performance of the transverse ventilation system. To that purpose, we investigated the extent of the backflow length downstream of the dampers, the "confinement velocity" (suppressing the back-layering flow downwind of the vents) and the stability of the smoke stratification. The results show that the best performances are achieved when the width of the dampers is the same as the tunnel width: this minimises the extent of the back-layering flow (for given extraction flow rates) and ensures the stability of the smoke stratification. The worst conditions are observed with square-shaped dampers located on the side of the ceiling, this configuration disturbs the stratification of the smoke layer before the confinement conditions are reached. Subsequently, we evaluated the effect of solid barriers -placed on the tunnel ceiling downstream of same three dampers typologies- on the propagation of the smoke. The results show that these barriers improve significantly the efficiency of system with square-shaped dampers located on the side of the ceiling: they reduce the confinement velocity and enhance the stability of the smoke stratification.

Keywords: Road tunnel safety, Smoke control, Transverse ventilation, Buoyant plume, Back-layering, Confinement velocity, Solid barriers.

Nomenclature

H	Height of the tunnel (m)
W	Width of the tunnel (m)
h	Height of the barrier (m)
D_i	Diameter of the source (m)
L	Smoke back-layering flow length (m)
B_i	Buoyancy flux (m^4/s^3)
g	Gravity acceleration (m/s^2)
q	Volume flow (m^3/s)
ρ	Density (kg/m^3)
Q_c	Heat release rate of the fire (kW)
T	Temperature (K)
C_p	Specific heat at constant pressure (kJ/kg K)
U_0	Induced longitudinal ventilation velocity (m/s)
U_e	Extraction velocity (m/s)
W_i	Injection velocity of the gas mixture at the source (m/s)
$U_{0,c}$	Confinement velocity (m/s)
$U_{e,c}$	Extraction confinement velocity (m/s)
A_d	Cross-sectional area of an extractor vent (m^2)
V	Sensor output voltage (volt)
R_c	Confinement velocity ratio (-)
Fr_0	Longitudinal Froude number (-)
Fr_e	Extraction Froude number (-)

© 2019 published by Elsevier. This manuscript is made available under the CC BY NC user license
https://creativecommons.org/licenses/by-nc/4.0/

$Fr_{0,c}$ Confinement Froude number (-)
$Fr_{e,c}$ Extraction confinement Froude number (-)
Ri Tunnel Richardson number (-)
Γ_i Plume Richardson number (-)
α Plume entrainment coefficient (-)
Ls Left side of the tunnel (-)
Rs Right side of the tunnel (-)
P_d Position of the dampers (-)
S_d Shape of the dampers (-)

Subscripts

$_0$ Property of the ambient condition
$_i$ Property of the plume at the source
$_{he}$ Helium Properties
$_e$ Property of the flow at the exhaust vents
$_r$ Property of the flow in the rotameter

Acronyms/ Abbreviations

HRR Heat Release Rate
FDS Fire Dynamics Simulator
RSD Rectangular-Shaped Damper
SSD-PC Square-Shaped Damper Placed in the Centre of the tunnel ceiling
SSD-PS Square-Shaped Damper Placed in the Side of the tunnel ceiling
ACH Air Changes per Hour

1 INTRODUCTION

The consequences of an event such as a fire or an accident in confined spaces such as a tunnel can be tragic. In these structures, due to the components and materials of the vehicle (plastics, tires, etc.) as well as all hazardous substances transported (fuel, wood, textile, plastic, etc.), fires can produce a large amount of toxic smoke. This smoke causes a loss of visibility that can prevent the evacuation of users who end up inhaling harmful gases and toxic substances. The smoke is indeed the major source of death in tunnel fires. Therefore, the installation of safety systems is imperative to ensure good safety conditions for tunnel users and emergency services in case of fire. Ventilation is one of the most important systems for fighting fires and controlling the dispersion of toxic smokes in these spaces. Based on traffic mode (i.e. one-directional or bi-directional) and flow regime (i.e. congested or uncongested) in the tunnels, two types of mechanical ventilation can be defined: longitudinal and transverse ventilation systems.

Longitudinal ventilation is required for road tunnels with unidirectional low traffic and is designed to produce a longitudinal flow in the same direction as vehicle traffic (Fig. 1a). With this strategy smoke and combustion products are pushed downstream of the fire source location to ensure the safe evacuation of people located upstream of the fire and to facilitate the intervention of rescue forces. Transverse ventilation systems are instead suitable for long bidirectional tunnels or congested unidirectional traffic tunnels (Fig. 1b). These are cases in which longitudinal ventilation is not suitable because, in these cases, pushing the smoke in one direction can endanger the tunnel users. With transverse ventilation, the smoke is extracted through dampers, which are generally located on the ceiling, whilst controlling the longitudinal air flow in the tunnel. Two objectives are generally pursued: the preservation of the natural stratification and the confinement of the smoke within a limited section of the tunnel, in which the extraction takes place.

a)

b)

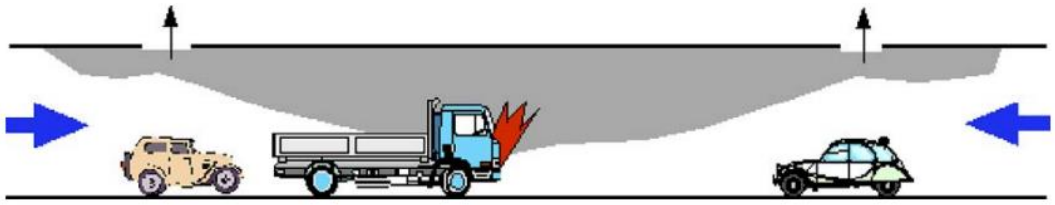

Fig. 1. **a)** Fire-induced smoke longitudinal control [1]. **b)** Fire-induced smoke transverse control [1].

While the smoke control in longitudinal ventilation has been the subject of extensive research [2-5], the literature is much scarcer regarding transverse ventilation. In this latter strategy, a main flow control parameter is referred to as 'the confinement velocity', defined as the minimum adverse velocity required to prevent the smoke from propagating beyond the extraction dampers, and the associated extraction flow rate at the ceiling vents. Vauquelin and Mégret [6] conducted fire experiments in a small-scale tunnel equipped with two mechanical exhaust ducts located one on either side of a fire source to study the influence of their location and their shape on the exhaust system efficiency for different fire heat release rates (HRR). They concluded that a duct with the transverse rectangular shape located at the tunnel ceiling is more efficient than the other ducts tested, whatever their shape and location. Vauquelin and Telle [7] performed another experimental study with a single vent activated downstream of the source (and assuming that smoke flow would be symmetrical with respect to the fire location). They evaluated the stratified smoke layer length downstream of the vent and the confinement velocity, for several values of HRR. Vauquelin [1] then performed other experiments with the same experimental set-up, but with a two vents system, to estimate the extraction flow rate required for a given HRR. Wang et al. [8] carried out a series of full-scale burning experiments in tunnel with roof openings to study the effect of natural smoke exhaust on the behaviour of smoke propagation, velocity and temperature fields under the ceiling, height of smoke layer and backflow distance. Due to the high costs and the difficulties inherent when conducting such fire experiments in a real tunnel, they extended this study by performing numerical simulations to include other fire scenarios with various vertical shaft arrangements on tunnel roof [9]. Ingason and Li [10] conducted a series of small scale fire experiments to investigate the efficiency of a single extraction system and a two-point extraction system. They concluded that the induced longitudinal velocity required to confine all smoke is low in the case with two-point extraction system. Fan et al. [11] conducted experimental simulations of fires in a tunnel equipped with a vertical shaft to quantify the effect of plug-holing on the smoke exhaust efficiency under natural ventilation. Their results showed that a high mixing process between the hot smoke layer and the cold air layer occurs because of the stack effect inside the shaft. Li et al. [12] used the Fire Dynamics Simulator (FDS) software to study the plug-holing phenomenon that occurs under the mechanical smoke exhaust in a tunnel when fresh air is drawn directly into the smoke extraction system from the bottom layer. This phenomenon is undesirable and should be avoided as it greatly reduces the efficiency of smoke extraction in tunnel fires [1, 13-17]. In recent years, further experimental [18-21] and numerical [22-24] studies investigated the performance and efficiency of extraction systems on smoke control in the case of a fire focusing on the vent size and fire source location [22], the tunnel slope [20], the location and shape of the exhaust vents [6].

The ventilation of road tunnels can be also controlled by combining both ventilation systems, transverse and longitudinal, an approach that has been recently considered in the tunnel ventilation literature. Lee et al. [25] conducted fire tests in a small-scale tunnel to evaluate the performance of the smoke extraction duct under natural and longitudinal ventilation flow conditions. Their results showed that the efficiency of the smoke extraction through the dampers is better with natural ventilation than with longitudinal ventilation, because of the preservation of the smoke stratification in the tunnel. Chen et al. [26] carried out experiments in a reduced-scale tunnel to study the effect of the distance between ceiling extraction and heat source on thermal buoyant smoke back-layering length in a tunnel with combination of longitudinal ventilation and ceiling extraction opening at the downstream side only. They found that the smoke back-layering length increases with increasing distance between the ceiling extraction opening and the heat source. Yao et al. [27] considered the case with a vertical shaft

upstream of the fire source to investigate the length of the smoke back-layering flow in longitudinal ventilated tunnel fires. Their experimental results showed that the vertical shaft can considerably reduce the smoke back-layering flow length (compared to the tunnel without a vertical shaft). In the same small-scale tunnel previously used by Chen et al. [26] and with the same ventilation system, Tang et al. [28] carried out a series of experiments to investigate the behaviour of the buoyant smoke flow stratification. They found that the combination of both ventilation systems had a strong influence on the smoke stratification and the flow configuration could be classified into different regimes.

In this study, we present the results obtained in the experimental analysis of smoke control using transverse ventilation in a scale model tunnel. The fire smoke in the tunnel is modelled by the continuous release of a light gas (mixture of air and helium), a method which has been consolidated through the study of the critical velocity and back-layering phenomenon [29-30]. The smoke is extracted through two mechanical exhaust vents located on the ceiling of the tunnel, one on each side of the source and equidistant from the buoyancy source. As already mentioned, the confinement velocity is defined as the minimum induced longitudinal velocity required to prevent the smoke from flowing downstream of the vent. When the induced longitudinal velocity is lower than the confinement velocity, a smoke backlayering flow appears downstream of the exhaust vent. The back-layering length is measured between the downstream edge of the exhaust vents and the extremity of the smoke backlayer. We test two different shapes of the extraction dampers, a square shape and a transverse rectangular shape (Fig. 3). The two dampers have the same cross-sectional area and the rectangular damper extends across almost the whole width of the tunnel (Fig. 3a). The square-shaped exhaust vent is placed on the ceiling in two different locations: firstly in the centre of the ceiling (Fig. 3b) and the secondly on one of the ceiling edges (Fig. 3c), over a width about one-third the tunnel width. Our work focuses on the measurement of smoke back-layering lengths, the determination of confinement velocities and the potential provision of qualitative information on stratification according to the source conditions and the extraction flow rates. The aim is to compare the results obtained with the different exhaust vents in order to evaluate the influence of the previously defined parameters (i.e. shape and location of the extraction dampers) on the performance of the smoke extraction system. Once this analysis has been carried out, we test the effect of the solid screens on the smoke confinement by fixing barriers to the tunnel ceiling, one downstream of each damper. In full scale tunnel, these barriers are designed to be mobile and would be deployed in the event of fires only. The influence of these barriers on the propagation of buoyant smoke in the tunnel with a longitudinal ventilation has already been studied [31]. The results showed that the large barriers prevent the smoke back-layer downstream of the source even at low ventilation velocities. The goal here is to examine their effects on the confinement velocity as well as on the stratification of the buoyant smoke layer in order to determine if they can improve the efficiency of the smoke extraction system.

2 EXPERIMENTAL SET-UP AND MEASUREMENT TECHNIQUES

2.1 The reduced scale model

Fire simulation experiments are carried out in a 1/25 reduced-scale model tunnel developed at the Laboratoire de Mécanique des Fluides et Acoustique (LMFA) at the Ecole Centrale de Lyon (Fig. 2a). A schematic view of the experimental setup is presented in Fig. 2b. The model tunnel is a channel with a rectangular cross-section. It is 8.4 m long, 0.36 m wide and 0.18 m high. Fire-induced smoke is simulated by a release of a light gas, a mixture of air and helium, into ambient air. The air and helium flow rates are controlled and measured using two flow meters. Both gases are well mixed in a long pipe and seeded with nebulised oil before being injected in the plenum. The air flow used to seed the oil particles, controlled by a flowmeter, is low so as not to influence the density of the mixture [35]. The mixture is then injected through a circular source of diameter D_i = 0.1 m placed at the centre of the tunnel at ground level. The side wall of the tunnel is made of transparent toughened glass, enabling visualisation of the buoyant fluid (seeded with particles) on a two-dimensional longitudinal plane illuminated by a laser beam emitted from a lens located at the inlet box of the tunnel.

a)

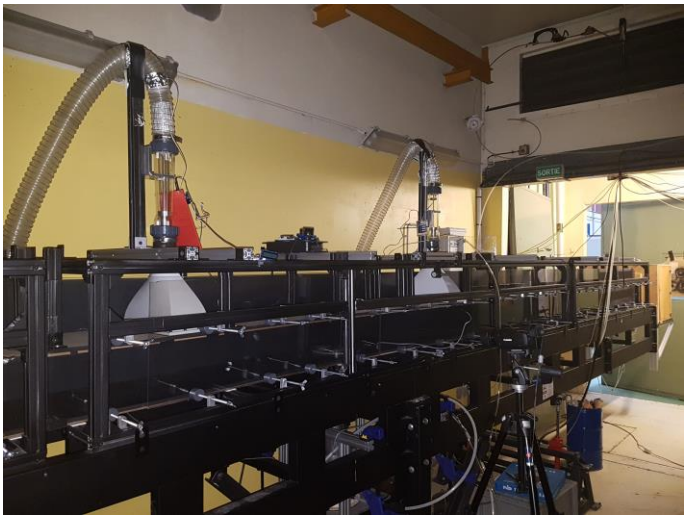

b)

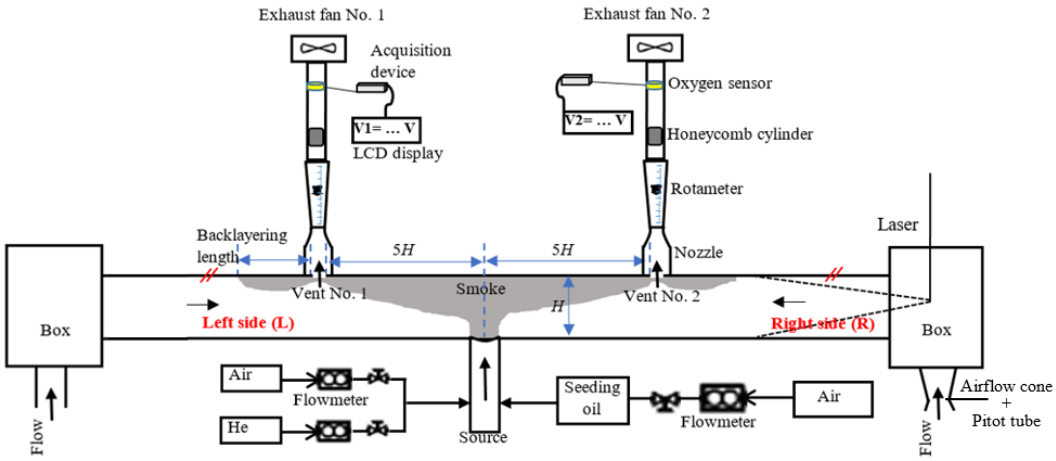

Fig. 2. Experimental setup with transverse smoke control system. **a)** A real picture of the setup. **b)** A schematic of the setup.

The tunnel is equipped with two dampers placed on the ceiling, one on each side and set the same distance from the source (i.e. 5*H*, *H* is the height of the tunnel). Each of them is connected to a mechanical exhaust fan. Both fans are remotely controlled and their rotation speed is easily adjusted by means of a potentiometer wired to each of them. Each fan produces an extraction airflow in the range 5 - 150 m^3/h. Assuming a tunnel of infinite length with dampers located at a distance of 10H, by taking as reference the volume of the area between each two exhaust vents (i.e. $10H$ x H x $2H \approx 0.117$ m^3), the extraction rate produced by each fan in terms of "air changes per hour (ACH) " ranges from about 43 to 1286 ACH.

Two different forms of dampers were used to carry out these experiments, a square shape "SSD" (Fig. 3b and Fig. 3c) and a transverse rectangular shape "RSD" (Fig. 3a) with an identical surface area of about 0.011 m^2. Their dimensions are 0.104 m x 0.104 m and 0.32 m x 0.034 m, respectively. Two different positions of the square-shaped dampers were tested, the first position in the centre, referred to as "SSD-PC" (Fig. 3b), and the second on one of the sides of the tunnel ceiling, referred to as "SSD-PS" (Fig. 3c).

The dampers are designed to be easily installed in the tunnel ceiling with fixed connections (8 screws). On each side, a rotameter (see § 2.3) with a range 6.4 - 64 m^3/h (and from 16 to 160 m^3/h for high flow rates) is used to measure the extraction flow rates through the exhaust duct. The nozzle placed between the damper and the rotameter particularly helps to ensure a uniform flow velocity at the rotameter entrance in order to avoid fluctuations of the rotating float inside the

rotameter. The position of the float on a linear scale indicates the flow rate passing through the rotameter. However, the density of the smoke flows is lower than that of the air and a correction of the flow rates measured according to their densities is therefore required. For this purpose, a calibrated oxygen sensor is placed above each rotameter to measure the concentration of air within the exhaust smoke flow. A honeycomb cylinder is placed before the oxygen sensor to protect it from oil particles that could degrade its measurements.

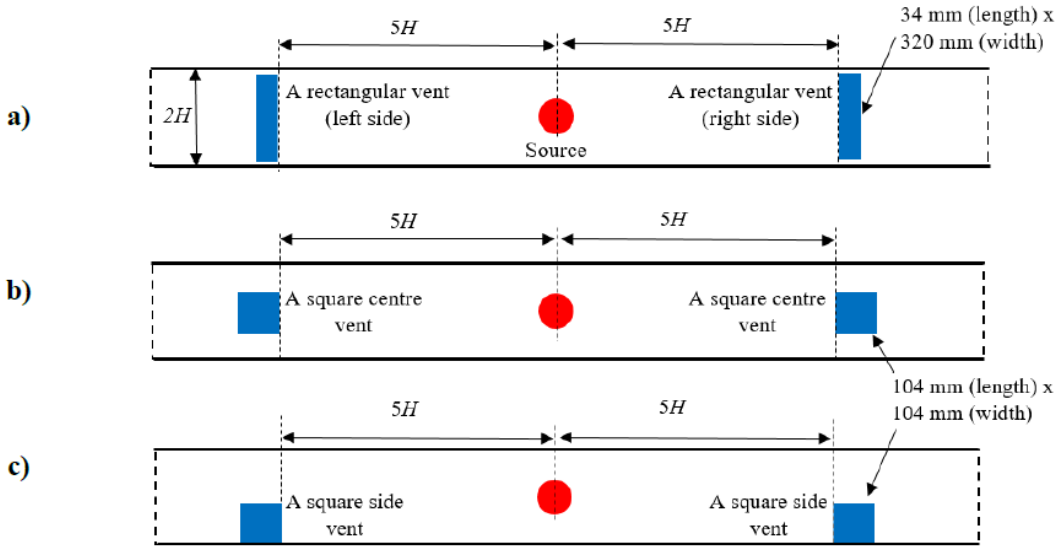

Fig. 3. Schematic top view of the different exhaust vents with their location on the tunnel ceiling. **a)** Exhaust vent with transverse rectangular shape (RSD). **b)** Exhaust vent with square shape placed in the centre of the tunnel ceiling (SSD-PC). **c)** Exhaust vent with square shape placed on the sides of the tunnel ceiling (SSD-PS).

To study the effect of barriers on the propagation of the smoke, two large barriers used in our recent work [31] were considered. Their heights are $h = H / 4$ and $h = H / 3$ and their widths are equal to the width of the tunnel. The barriers are solid to withstand the smoke flow forces and the induced longitudinal airflow forces. For each case of dampers, two barriers are fixed to the ceiling of the tunnel, one on each side of the source. The barriers (which are transparent to allow the smoke to be visualised) are located just downstream of the dampers, as is shown in Fig. 4. The idea is to evaluate the additional benefits they can offer to improve the efficiency of transverse ventilation systems, by comparing the results obtained with and without barriers. Note that in real tunnels, these barriers are designed to be mobile and will only be deployed in the instance of a fire.

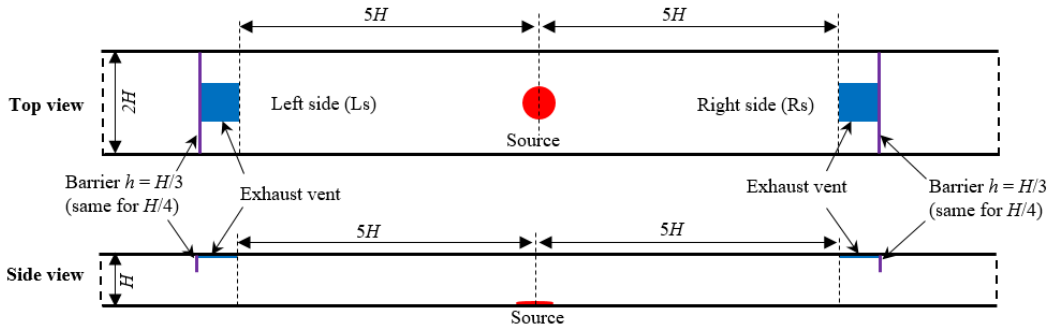

Fig. 4. Diagram of the experimental setup with large barriers ($h = H / 3$) fixed to the tunnel ceiling just upstream of the dampers (in this case, the exhaust vents are represented by square-shaped dampers placed in the centre of the tunnel ceiling, the same is applied for other types of dampers and for the barrier of height $h = H / 4$).

2.2 Flow control parameter and similarity

As customary in small scale experiments, the fire source within the tunnel is modelled by means of the injection of light gas, a mixture of helium and air [32, 33]. As shown by Jiang et al. [32] in experiments with longitudinally ventilated tunnel, these densimetric plumes can be considered to reliably reproduce the smoke behaviour produced by a fire, provided that the size of the flames does not exceed the tunnel half-height. Of course, adopting this approach, we will fully neglect any dynamic and thermal effect induced by heat transfers from conduction at the tunnel walls or by radiation [1].

We consider a flow in an infinitely long tunnel equipped with a transverse ventilation system while fixing the geometrical parameters of the tunnel (the height H and the width W). We can assert that the extension L of the smoke back-layer could depend on the source parameters (i.e. the diameter of the source D_i, the velocity W_i and the density ρ_i of the buoyant gas release) and on the induced longitudinal velocity U_0 [30, 34], as well as on the geometrical parameters of the exhaust vents (i.e. the cross-sectional area A_d, the shape S_d and the position P_d). Adopting basic dimensional arguments [32, 33], assuming negligible diffusive effects, the dimensionless length of the back-layer can then expressed as:

$$\frac{L}{H} = f\left(\Gamma_i, \frac{\rho_i}{\rho_0}, \frac{D_i}{H}, \frac{U_0}{W_i}, \frac{A_d}{H^2}, S_d, P_d\right), \quad (1)$$

where ρ_0 is the ambient air density and $\Gamma_i = \frac{5}{4\alpha\pi}\frac{B_i}{D_i W_i^3}$ is the "plume Richardson number", with $\alpha = 0.12$ (a reference value for the 'top-hat' entrainment coefficient [36] and where

$$B_i = g q_i \frac{\rho_0 - \rho_i}{\rho_0}, \quad (2)$$

is the buoyancy flux, with g the gravitational acceleration and q_i the total volume flow of the mixture at the source. Note that the buoyancy flux B_i can be directly linked to an equivalent heat release rate (Q_c) by the relation:

$$Q_c = B_i \left(C_p \rho_0 T_0\right)/g, \quad (3)$$

where T_0 is the ambient air temperature and C_p is the specific heat capacity (assumed constant).

Since the confining velocity $U_{0,c}$ is defined as that inducing a null back-layering length, from (Eq. 1) we can write

$$\frac{U_{0,c}}{W_i} = f\left(\Gamma_i, \frac{\rho_i}{\rho_0}, \frac{D_i}{H}, \frac{A_d}{H^2}, S_d, P_d\right) \quad (4)$$

Previous studies [30, 35] have shown that, considering highly buoyant releases, i.e. for $\Gamma_i > 1$, the relations (Eq. 1) and (Eq. 4) can be highly simplified. In these conditions the back layering length and the confinement velocity do not show any clear dependence on single source parameter, such as the diameter of the source D_i and the density ρ_i and exit velocity W_i of the buoyant gas release. These parameters affects the flow instead only as far as they induce variations in the source buoyancy flux B_i (Eq. 4). In these conditions (Eq. 1) therefore reduces to:

$$\frac{L}{H} = f\left(Fr_0, \frac{A_d}{H^2}, S_d, P_d\right) \quad (5)$$

with $Fr_0 = U_0/(B_i/H)^{1/3}$ a Froude number, which expresses the ratio between the inertia forces induced by the ventilation flow and the buoyancy forces induced by the injection of the buoyant plume at the source. The relation (Eq. 5) is sometimes [30] presented as a function of "tunnel Richardson number" $Ri_0 = \frac{B_i}{{U_0}^3 H} = {Fr_0}^{-1/3}$. If we further assume that cross-sectional area A_d is unaltered we finally obtain that:

$$\frac{L}{H} = f(Fr_0, P_d, S_d) \quad (6)$$

Which implies that the critical Froude number

$$Fr_{0,c} \propto U_{0,c}/(B_i/H)^{1/3} = \text{constant} \quad (7)$$

is a function of the shapes and positions of the extractor vents, i.e. that

$$Fr_{0,c} = f(P_d, S_d) \quad (8)$$

The determination of the dependences expressed by (Eq. 6) and (Eq. 8) constitutes the object of our study.

Note that from (Eq. 7) we have that the confinement velocity can be related to the buoyancy flux as $U_{0,c} \propto B_i^{1/3}$ (which means that the fire plume is only characterised by its buoyancy flux) and therefore to the heat release rate as $U_{0,c} \propto Q_c^{1/3}$.

2.3 Calibration of rotameters and oxygen sensors

The rotameter is a device used to measure the volumetric flow rate of fluid, it consists of a tapered tube with a rotating float inside that is pushed up by the drag force of the flow and pulled down by gravity. Since the drag force depends on the fluid density, for our purposes, the flowmeter scale requires a calibration to take into account the variation of the density of the gas, providing the relationship between the flow rate (indicated by the rotameter) for a reference air density and the actual flow rate, for any gas mixture. For this purpose, tests were carried out in another experimental set-up (Fig. 5), made up of: two flow meters to independently control air and helium flows; a long pipe to ensure a good mix of air and helium, a rotameter for flow measurements, two oxygen sensors to measure the concentration of oxygen in the gas mixture.

The tests were carried out for varying density ratios ρ_i/ρ_0 = 0.5, 0.6, 0.7, 0.8, 0.9 and 1. For each of these values of the density ratio, the calibration of the rotameter is performed with mixing rates (q_i) ranging from 130 L/min to 700 L/min (i.e. 8 m^3/h to 42 m^3/h). The density of the gas mixture is estimated by measuring the oxygen concentration by means of electrochemical sensors placed downstream of the rotameter. This concentration is associated to a voltage value, it is acquired by an Arduino board (ARDUINO UNO - DIP REV3) and displayed on a digital screen (Grove - LCD RGB Backlight). Two rotameters with different measuring ranges of 6.4-64 m^3/h and 16-160 m^3/h were calibrated. Only the latter has actually been used in our experiments.

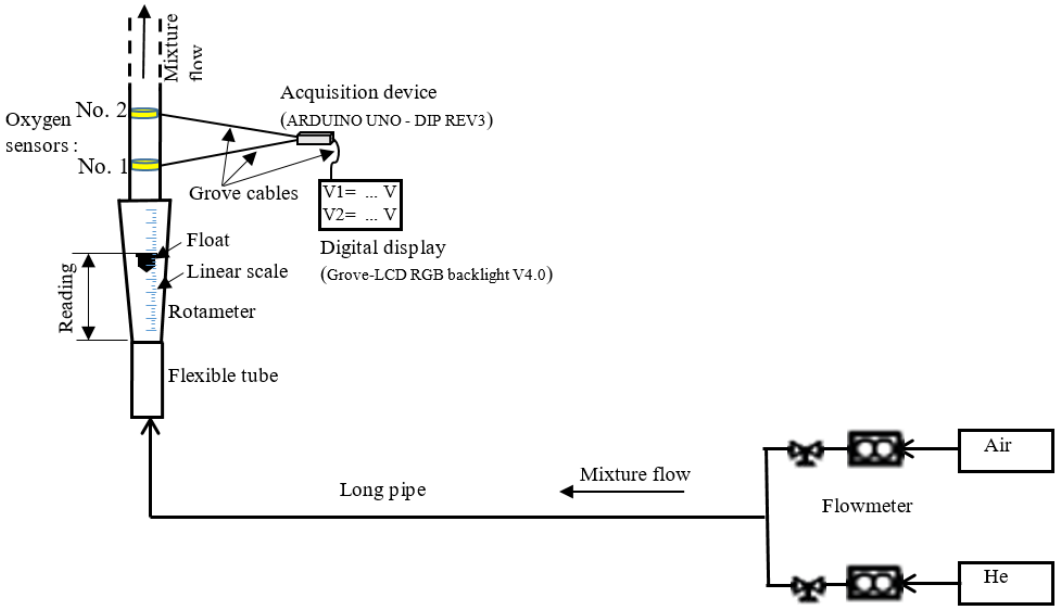

Fig. 5. Experimental set-up for calibration of rotameters and oxygen sensors.

Fig. 6 shows the relationship between the flow rate provided by the rotameter (q_r) and the actual flow rate (q_i). Fig. 6a and Fig. 6b show the results of the rotameter with measuring ranges of 6.4 m^3/h to 64 m^3/h and 16 m^3/h to 160 m^3/h, respectively. A linear fit of the data is performed for each density ratio and a correlation is obtained in the form: $q_r = \beta * q_i$ where β is a constant, whose value depends only on the density of the gas mixture (it decreases with decreasing gas density). From these data we can plot the curve corresponding to any density ratio between 0.5 and 1 by a simple linear interpolation.

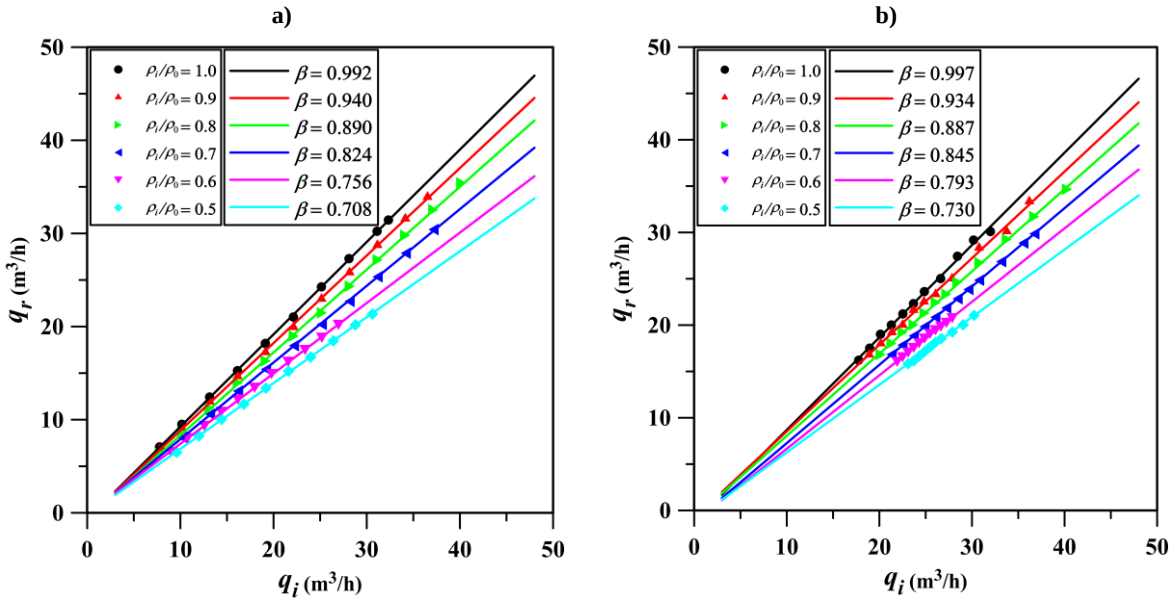

Fig. 6. The dependence between the measured flow rate q_r and the prescribed flow rate q_i for $0.5 \leq \rho_i/\rho_0 \leq 1$. '$\beta$' is the linear correlation factor between q_r and q_i. **a)** Rotameter with a range: 6.4-64 m^3/h. **b)** Rotameter with a range: 16-160 m^3/h.

Fig. 7 shows the results on the oxygen concentration measured by both sensors depending to the density of the mixture. With the type of sensor used in these experiments, we know the percentage of oxygen in the gas mixture (or in the ambient air) through the given output voltage of each sensor. Fig. 7a shows that the output voltage V_i increases with the density ρ_i and changes from one sensor to another. Fig. 7b shows the dimensionless voltage V_i/V_0 (V_0 is the output voltage of each sensor measured in the ambient air) versus the dimensionless density ρ_i/ρ_0. The two curves are similar, we can then conclude that both sensors have the same voltage response.

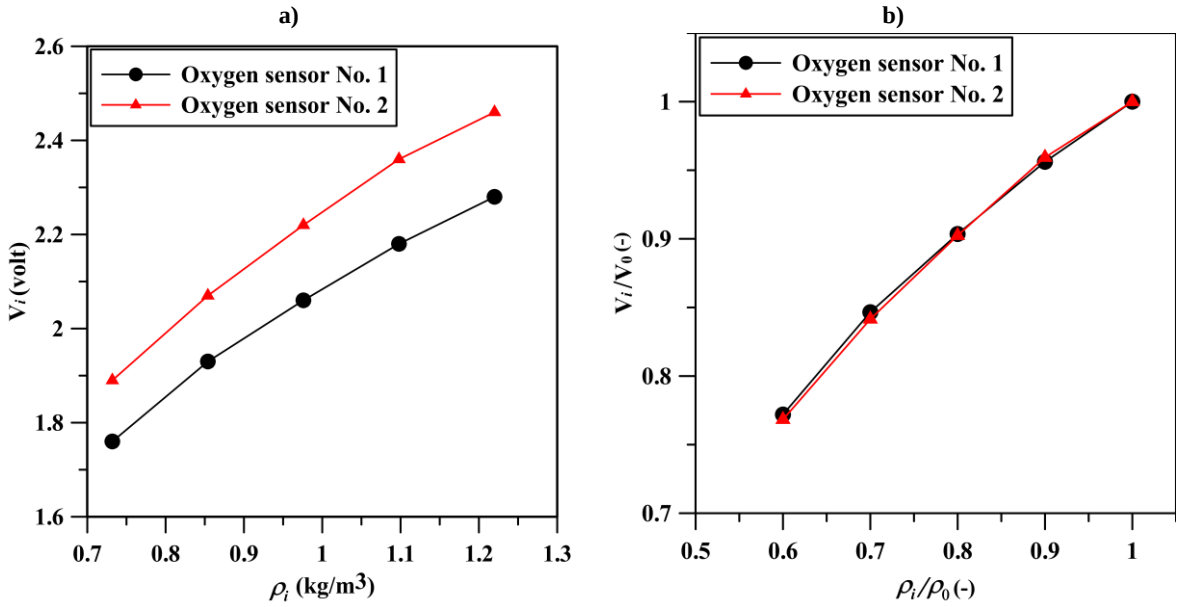

Fig. 7. Variation of the oxygen concentration measured by the two sensors (expressed in Volt) against the density of the mixture. **a)** The voltage V_i versus the density ρ_i. **b)** The dimensionless voltage V_i/V_0 versus the dimensionless density ρ_i/ρ_0.

From the two output voltage curves plotted in Fig. 7a, the density of the gas mixture in the two exhaust ducts can therefore be obtained. Knowing the density of the extraction smoke, the actual flow corresponding to that measured by each rotameter is obtained using the curves (or interpolation curves) plotted in Fig. 6.

2.4 Experimental protocol

Experiments were performed for a fixed density ratio ρ_i/ρ_0= 0.7, a fixed source diameter D_i/H = 0.56, and a plume Richardson number in the range $1 \leq \Gamma_i \leq 40$. With these conditions, the average injection velocity (W_i) at the source varies from 0.13 m/s to 0.73 m/s, the buoyancy flux (B_i) is between $3*10^{-3}$ m^4/s^3 and $2*10^{-2}$ m^4/s^3 (and the corresponding heat release rate (Q_c) is between 0.11 kW and 0.71 kW in this reduced scale model).

The average extraction velocities through the dampers (U_e) were calculated by dividing the extraction flow rate (once they are determined and corrected to the fluid density) by the cross-sectional area of the damper. As shown in Fig. 2b, the tunnel is equipped with a pitot tube at one end to estimate the ventilation flow rate. However, for most of the experiments, the ventilation flow rate was too low to be measured by this system. Therefore the longitudinal induced velocity U_0 and the relative air flow q_0 are estimated by a mass balance (assuming that the flow is perfectly symmetric with respect to the source position) as (see Fig. 8):

$$q_0 = \frac{\rho_e}{\rho_0} q_e - \frac{\rho_i}{\rho_0} \frac{q_i}{2} \qquad 9$$

where $q_0 = q_{01} = q_{02}$, $q_e = q_{e1} = q_{e2}$ and ρ_e is the density of the extraction smoke flow. Note that the symmetry of the flow has been verified, for a given range of airflow, by directly measuring the longitudinal velocities with a Pitot tube and comparing them to those calculated with Eq. 9.

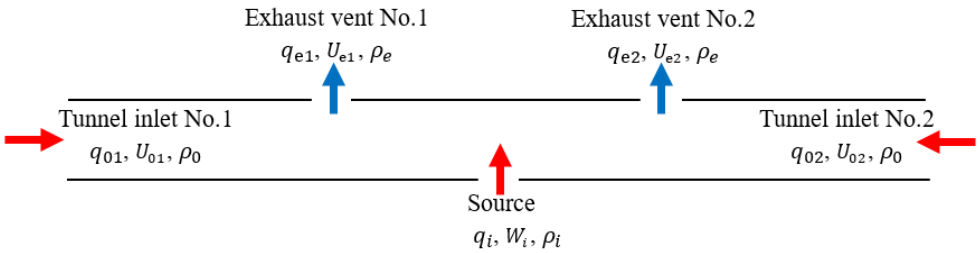

Fig. 8. Schematic view of all input and output flows in a tunnel with two extraction points.

To ensure a symmetrical dispersion of the smoke flow in the tunnel with respect to the location of the source, the two exhaust fans must be controlled simultaneously and their power adjusted to impose the same flow on both sides. In this way, using flow visualisation and camera recordings, we can then measure the smoke back-layering lengths, determine the confinement velocities according to the source conditions, and report qualitative information about the stratification of the smoke layers in the tunnel with and without barriers. By regulating the power of the exhaust fans, we could set the front of the back-layering flow at the position of the extraction dampers, at the confinement conditions, characterised by a "confinement velocity" $U_{0,c}$ within the tunnel, and to an associated extraction confinement velocity $U_{e,c}$. Fig. 9 shows an example of smoke visualisation in the tunnel with rectangular exhaust vents for two different ventilation velocities. In case of a ventilation flow lower than the confinement condition (with U_{e1}= 0.52 m/s and U_{e2}= 0.50 m/s and U_{01}= 0.069 m/s and U_{02}= 0.063 m/s), a stratified smoke layer develops downstream of the exhaust vents (Fig. 9a). The smoke layer is stable and symmetrical with respect to the position of the source, its length is equal to twice the tunnel height (i.e. L/H = 2).

By increasing the extraction flow rate of the two fans (Fig. 9b), the longitudinal velocity of the induced fresh air increases and the back-layering length downstream of the exhaust vents decreases progressively on both sides, until reaching confinement ventilation conditions (i.e. L/H = 0), here obtained for $U_{e1,c} = U_{e2,c}$ = 0.58 m/s and $U_{01,c} = U_{02,c}$ = 0.08 m/s.

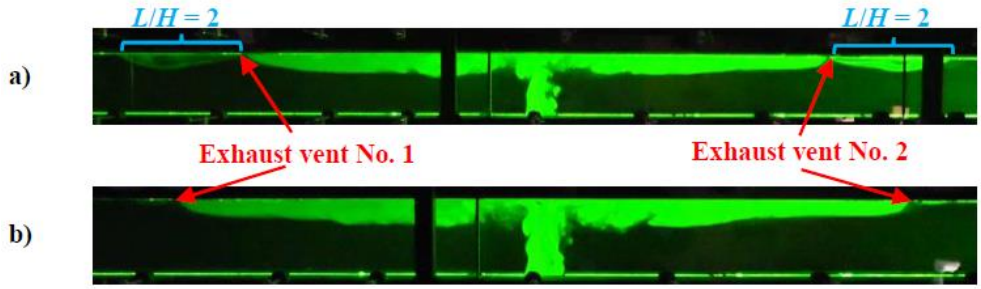

Fig. 9. Smoke visualisation in the tunnel with a two-point transverse extraction system (rectangular dampers, Γ_i=8). **a)** Non-confinement ventilation conditions: smoke back-layer appears downstream of the dampers. **b)** Confinement ventilation conditions: smoke backflow is completely suppressed.

3 RESULTS AND DISCUSSIONS

3.1 Smoke backflow length

Measurements of the smoke back-layer lengths downstream of the dampers were performed for given source conditions (D_i/H = 0.56, ρ_i/ρ_0= 0.7 and Γ_i = 8). The flow rate of the two exhaust fans was first set to the minimum, then increased gradually. For each ventilation flow condition, the backlayer length downstream each of the two extraction vents and the corresponding extraction flow rates were recorded. Note that the uncertainty on the estimate of the flow rates with the rotameters is approximately ±1 m^3/h, while the uncertainty on the smoke length measurement is approximately ± H/2. The results obtained for different shapes and locations of the exhaust vents are presented in Fig. 10. For all cases, the dimensionless backflow lengths L/H measured on both the left and right sides of the tunnel are plotted against the extraction Froude number $Fr_e = U_e/(B_i/H)^{1/3}$ in Fig. 10a and against the longitudinal Froude number $Fr_0 = U_0/(B_i/H)^{1/3}$ in Fig. 10b. As expected (Eq. 9**)**, the relationship between U_0 and U_e is linear (as well as between Fr_e and Fr_0), and each curve shown in Fig. 10a has the same trend as its corresponding curve in Fig. 10b. The results show that the backflow length decreases with the increase of the Froude number. For each type of exhaust vent and for a fixed value of Froude number, the back-layering length on the right side (Rs) of the tunnel is greater than that measured on the left side (Ls). This is because the inlet flow at the two tunnel entrances are asymmetric, resulting in uneven distribution of head losses. However, for a reduced backlayering length (i.e. $L/H \leq 1$), the effect of these uneven head losses becomes negligible and the backflow becomes perfectly symmetrical (relative to the source location).

Two features can be distinguished from the comparison of the results obtained with dampers of square (SSD) and rectangular shapes (RSD): firstly, the length of the back-layer flow and secondly, on its correlation against the Froude number. With regard to the first point, for the same back-layering length, the Froude number is lower with the rectangular-shaped dampers than with the square-shaped dampers. This means that even though the cross-sectional area of the two shapes of dampers is the same, their efficiency in smoke extraction is different. Concerning the second point, the evolution of the backflow length against the extraction velocity is different for the two different shapes. For rectangular-shaped dampers, the back-layering length decreases very rapidly with increasing smoke extraction rate. As shown in Fig. 10, the dimensionless length (L/H) is reduced from 14 to 0 for an extraction Froude number (Fr_e) increasing from 1.10 to 1.72 (i.e. from 0.13 to 0.22 for Fr_0). In this particular case of full-width dampers, the smoke propagation downstream of the exhaust vents can be controlled with relatively low extraction rates, while preserving the stratification of the smoke layers (as illustrated in the example of Fig. 9b). For square-shaped dampers (SSD), the development of smoke back-layer exhibits different regimes, depending on the value of the Froude number. The first regime is characterised by a significant decrease in the back-layering length, as well as by the asymmetry of the smoke backflow with respect to the source location (i.e. Ls and Rs curves are not identical). This behaviour can be clearly observed in Fig. 10 for $L/H > 1$. The second regime is characterised by the case when $L/H < 1$: the backflow becomes perfectly symmetrical relative to the source location and its length is only slightly affected by changes in the extraction flow rate. In this regime, as observed during flow visualisation experiments, the smoke backlayer is suppressed

for the extraction rate values that perturbs the stratification of the smoke layer, i.e. inducing a significant mixing between the ambient air layer and the smoke layer. Furthermore, for these high flow rates we observe the occurrence of a phenomenon called 'plug-holing', i.e. the extraction of a large amount of fresh air flowing through the smoke layer. This phenomenon is clearly undesirable since it reduces the effectiveness of transverse ventilation systems. Fig. 10 also shows that the position of the square-shaped dampers plays a major role in the smoke back-layering lengths. Indeed, with the same ventilation conditions, the length of the backflow measured in each side of the tunnel is larger with the vents located on the sides of the tunnel ceiling (SSD-PS) than with the vents in the centre (SSD-PC).

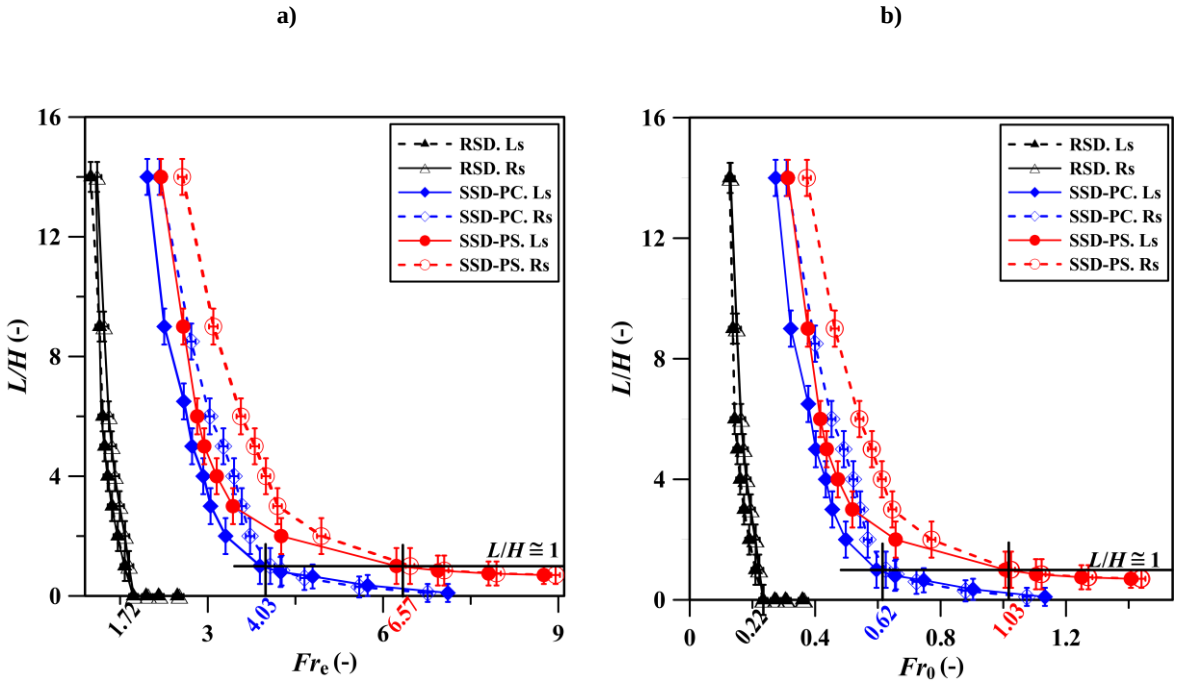

Fig. 10. a) Dimensionless back-layering length L/H against the extraction Froude number Fr_e. **b)** Dimensionless back-layering length L/H against the longitudinal Froude number Fr_0, for different shapes and locations of the exhaust vents.

The difference between the results obtained with the different dampers can be explained as follows: when the buoyant plume impinges the ceiling, the smoke layer extends in both longitudinal directions of the tunnel, it moves near the tunnel ceiling over its entire width. Once the smoke reaches the location of the vents, it is trapped by the full-width dampers, even at relatively low extraction rates. However, if the width of the dampers is much smaller than the width of the tunnel, only the smoke passing through the location of the exhaust vents is directly trapped, while the remaining smoke can flow downstream of the dampers through the remaining width of the tunnel (i.e. width not occupied by the dampers). To prevent this smoke from moving away from the vents, it is necessary to increase the induced longitudinal air flows on both sides of the tunnel. However, the extraction rates required with the vents located in the centre are significantly smaller than those needed with the vents placed on the sides.

Note that the non-dimensional density of the smoke measured by the sensors at the exhaust vents increases with the extraction flow rate for each of the three vent shapes investigated. The variation of ρ_e/ρ_0 was between 0.92 and 0.94 for the rectangular vents and between 0.95 and 0.98 for the square centre vents and square side vents (where ρ_e is the density of the smoke measured at the exhaust vents). This implies that, under the same source conditions, the higher the extraction rate the greater the proportion of ambient air extracted. In other words, the higher the value of ACH the lower the concentration of smoke in the extracted air. This also explains why the density ratios measured with the square vents are higher than those measured with rectangular vents. This is because the airflow needed to reduce or prevent the smoke back-layering with square vents is greater to that required for rectangular vents.

3.2 Confinement velocity

In principle, the confinement condition is reached when the smoke backflow downstream the damper is suppressed, i.e. for $L/H = 0$. However, as can be observed in Fig. 10, this condition is difficult to reach for the cases with square shaped dampers (SSD). In these cases the confinement conditions are therefore defined differently, i.e. as those inducing an extent of the backflow which is equal to the tunnel height, i.e. for $L/H = 1$, which will then be assumed as the reference length corresponding to the confinement velocity (a similar criterion was adopted by Vauquelin and Telle [7]). We therefore consider that the confinement condition will be attained when $L/H = 0$ (i.e. total confinement) for the rectangular shaped dampers (RSD) and when $L/H = 1$ for the square shaped dampers (SSD).

The study was performed with the different vents, the velocity measurements are taken from both sides of the tunnel (Ls refers to left side and Rs to the right side). The results on the confinement velocity are represented in Fig. 11a as a function of buoyancy flux, with the corresponding best-fit curves. The associated extraction confinement velocities and heat release rates are shown on the right y-axis and at the top x-axis of the graph. Fig. 11a shows that for each shape (or position) of dampers, the results for the two sides (curves Ls and Rs) are very similar to each other. Moreover, as expected, $U_{0,c}$ (as well as $U_{e,c}$) increases with increasing buoyancy flux B_i and therefore with increasing HRR. In all cases considered, the general dependence between these quantities can be expressed in the form $U_{0,c} = a\,{B_i}^{1/3} = b\,{Q_c}^{1/3}$ (similar with $U_{e,c}$), where 'a' and 'b' are proportionality constants whose values depend on the shape and the location of the dampers (they are low with RSD) as well as on other parameters not considered in this study, such as the shape and the aspect ratio of the tunnel cross section [4, 5], the size of the source [32, 34] and the distance between the source and the extraction points.

The confinement Froude number $Fr_{0,c}$ (as well as $Fr_{e,c}$) is estimated and plotted in Fig. 11b against the plume Richardson number Γ_i. As shown in the figure, this number does not depend on the source conditions (Γ_i), it is only related to the shape and position of the damper, which is in accordance with what is expected (Eq. 8). Its value is low with RSD ($Fr_{0,c}$ is around 0.22) and high with SSD-PS ($Fr_{0,c}$ is around 1.10). Note that this latter value exceeds that for a longitudinally ventilated tunnel [35] (which is of the order of unity). This proves that the square-shaped dampers placed on one side of the ceiling are not an effective means with which to control smoke propagation. Moving the dampers from the edge to the centre of the tunnel ceiling reduces the value of the confinement Froude number by approximately one-half and thus improves the efficiency of the ventilation systems.

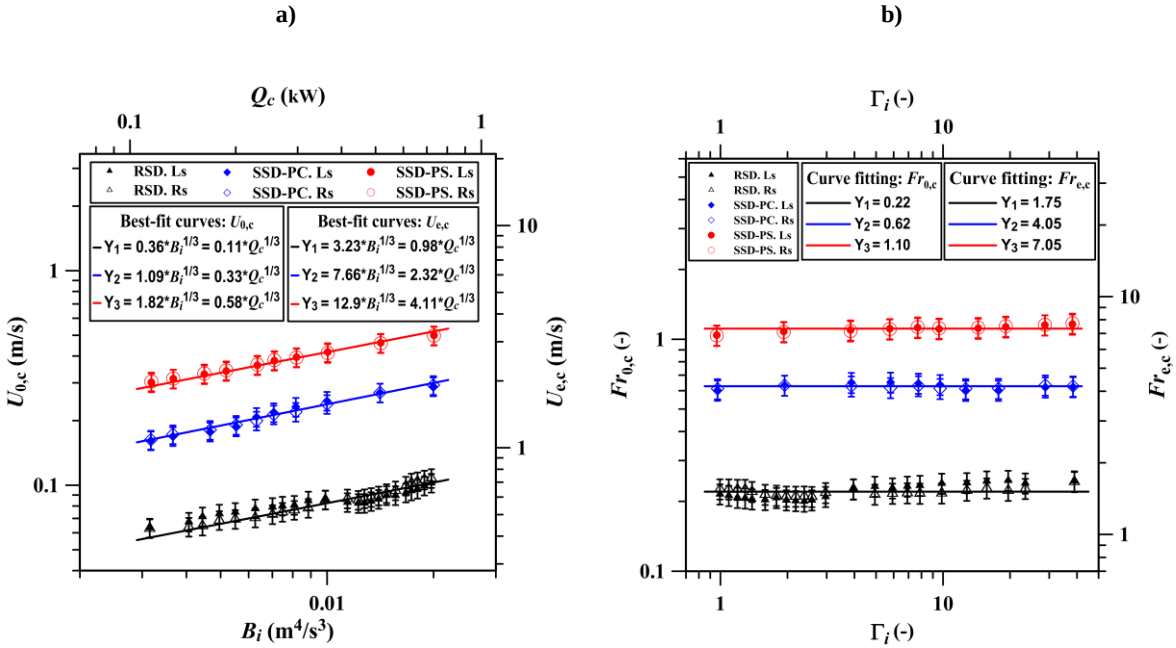

Fig. 11. a) The confinement velocity $U_{0,c}$ and the associated extraction confinement velocity $U_{0,e}$ against the buoyancy flux B_i and the associated heat release rate Q_c. **b)** The confinement Froude number $Fr_{0,c}$ and the associated extraction

confinement Froude number $Fr_{0,e}$ against the plume Richardson number Γ_i, for different shapes and locations of the exhaust vents.

It is worth noting that the results presented in Fig. 11 demonstrated that: i) the width of the damper is the relevant length scale for the smoke spread control in the tunnel with mechanical extraction systems, ii) the location of the damper relative to the centre of the tunnel plays a significant role in the confinement and extraction of smoke and iii) the confinement Froude number does not depend on the source conditions but only on the geometry of the exhaust vents.

It should be noted that, in confinement conditions, the density ratio (between the smoke and ambient air density) measured at the exhaust vents for each configuration increases with the plume Richardson number (i.e. with buoyancy flux and thus with the heat release rate). For $1 \leq \Gamma_i \leq 40$ (i.e. $3*10^{-3} \leq B_i(m^4s^{-3}) \leq 2*10^{-2}$), ρ_e/ρ_0 ranged from 0.91 to 0.97 with rectangular vents and from 0.96 to 0.99 with square vents. This can be explained by the fact that the higher the buoyancy flux (or the firepower), the higher the extraction rate, which causes a strong suction of the ambient air through the dampers. This means that the smoke concentrations in the extracted air decrease with increasing confinement values of ACH.

3.3 Effect of extraction rate on smoke stratification

Furthermore, we also focus on the stability of the smoke stratification within the tunnel. To that purpose, for each type of damper, the tests are performed with releases characterised by two values of Richardson number (Γ_i = 8 and Γ_i = 40) and a fixed density ratio 0.7. The procedure to investigate this effect is to increase (simultaneously) the flow rate of the two exhaust fans and at the same time observing the significant changes in the behaviour of the buoyant smoke flow. Images of these smoke behaviours are then recorded using a video camera and the flow regimes are expressed according to the Froude number Fr_0. The camera used is the "Canon LEGRIA HF G40". This includes an HD CMOS PRO sensor that provides a high-quality image of 2.07 mega pixels (i.e. an array of 1920 x 1080 pixels) along with precise 20 x optical zoom. The camera can be used to record outstanding high bitrate AVCHD 1080p video with variable frame rates.

3.3.1 Rectangular-shaped dampers (RSD)

Fig. 12 shows the behaviour of the buoyant smoke flow for different stratification regimes with rectangular-shaped dampers (only the right side of the tunnel is shown). Fig. 12a shows the smoke in confinement conditions (for $Fr_{0,c}$= 0.22). In this flow configuration, we can see the existence of two distinct layers, an ambient air layer at the bottom and a smoke layer at the top, without any exchange of particles between the two layers. Thus, we consider that stratification is well preserved and refer this to as a 'stable stratification' regime. The stratification remains relatively well-preserved until Fr_0 = 0.60, when a thin smoke appendix is formed below the exhaust vent (Fig. 12b). By further increasing the extraction rates, more ambient air is extracted through the exhaust vents and a larger amount of smoke is directed to the lower air layer (i.e. the plug-holing phenomenon). In this case, several vortices appear at the interface between the two layers, as well as in the lower air layer (Fig. 12c). Nevertheless, the visibility remains clear at the bottom of the tunnel. This configuration (i.e. when $0.6 \leq Fr_0 \leq 1.1$ approximately) marks the transition between a stable and unstable stratification regime. As the extraction rate increases further, the suction force increases, resulting in an increase in the induced longitudinal flow rate. The shear of generated instabilities induces the mixing between the upper and the lower fluid layers (see Fig. 12d). In this case, the whole area between the both vents is completely filled with smoke giving rise to a flow regime that we refer to as 'unstable'.

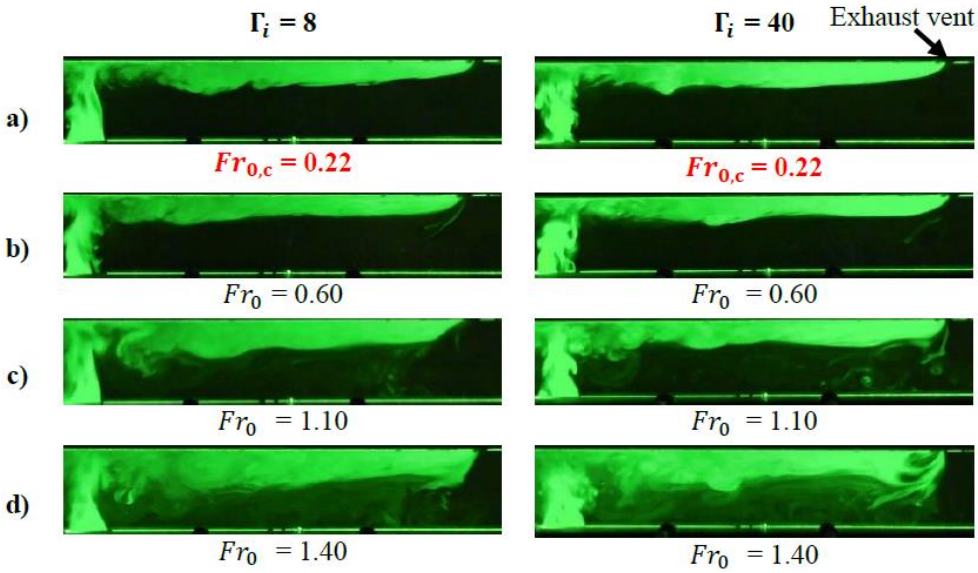

Fig. 12. Visualisation of the different stratification regimes of the buoyant smoke flow in the tunnel equipped with rectangular shaped dampers (RSD).

3.3.2 Square-shaped dampers positioned in the centre (SSD-PC)

Fig. 13 shows the flow visualisations for square-shaped dampers placed in the centre (SSD-PC). As previously mentioned (§ 3.2), the confinements conditions with the square-shaped vents are attained when the backflow downstream of the dampers becomes insensitive to the induced longitudinal air flow (i.e. for $L/H \approx 1$). The confinement Froude number is equal approximately to 0.60 (Fig. 13a). In this configuration, the stratification of the smoke layer is preserved. We can however notice the appearance of a small appendix (identical to that observed in Fig. 12b) at the bottom of the vents. This highlights the beginning of a transition between a stable stratification and an unstable stratification, which occurs for a Froude number identical to that estimated with rectangular-shaped dampers (i.e. Fr_0 = 0.60). By increasing the extraction flow rate, large smoke vortices are produced in the lower air layer (Fig. 13b), which we consider as representative of the unstable stratification regime. This happens for $Fr_0 = 0.80$, which is lower than that observed for the case of rectangular-shaped dampers (i.e. Fr_0 = 1.10). Fig. 13c and Fig. 13d show the configurations with a partial and complete de-stratification of the buoyant smoke layer. In these cases, the bottom of the tunnel is completely filled with smoke, therefore severely restricting the visibility.

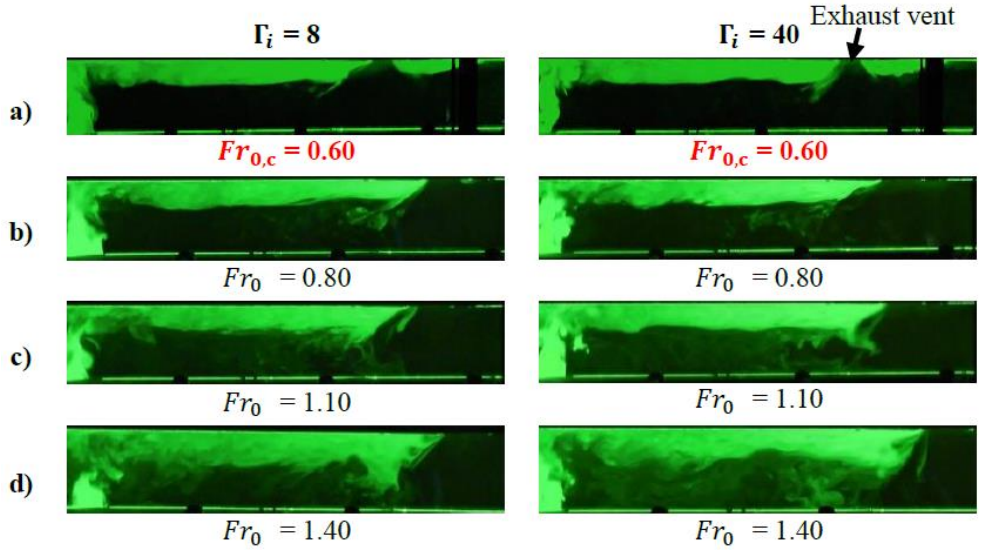

Fig. 13. Visualisation of the different stratification regimes of the buoyant smoke flow in the tunnel equipped with square-shaped dampers located in the centre (SSD-PC).

3.3.3 Square-shaped dampers positioned in the side (SSD-PS)

Fig. 14 shows the flow visualisations for square shaped dampers placed on one side of the tunnel ceiling (SSD-PS). We observe that: i) the vortices at the interfacial regions (see Fig. 14a) are well developed and clearly visible, due to the strong shear; ii) the smoke layer is slightly thicker than that observed in the previous case where the position of the vents is aligned on the same axis as the source location; iii) the stratification of the buoyant smoke layer is completely suppressed even before reaching the confinement conditions (see Fig. 14c), i.e. $Fr_{0,c}$ = 1.10. In summary, the smoke stratification pattern can be classified into three regimes identical to those observed with square shaped dampers located in the centre: stable stratification for a $Fr_0 < 0.6$, stable-unstable transition for a $0.6 \leq Fr_0 \leq 0.8$ and unstable for a $Fr_0 > 0.8$.

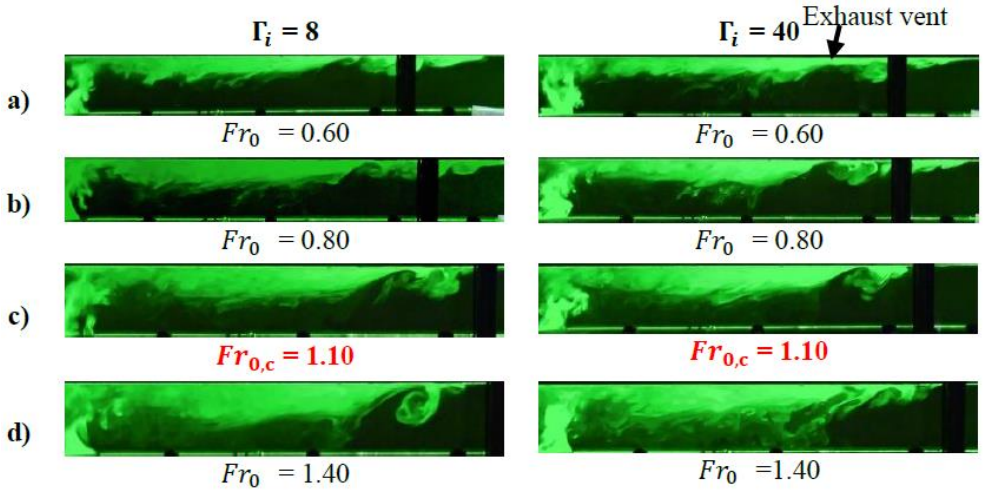

Fig. 14. Visualisation of the different stratification regimes of the buoyant smoke flow in the tunnel equipped with square-shaped dampers located on the side of the tunnel ceiling (SSD-PS).

Finally, it should be noted from Fig. 12, Fig. 13 and Fig. 14 that the smoke stratification behaviour for a constant Froude number is independent of the plume Richardson number (a similar smoke behaviour is observed with Γ_i = 8 and Γ_i = 40), however, it seems that this changes with the shape (or position) of the exhaust vents. This confirms that the Froude number is the only flow control parameter.

3.4 Effect of solid barriers on the propagation and behaviour of smoke

Our results show that the confinement conditions can be reached for flow rates that already induce a de-stratification of the smoke layer within the tunnel. It is therefore interesting to seek solutions to improve the efficiency of smoke extraction systems, i.e. the preservation of the stratification and the confinement of the smoke within a limited section of the tunnel, in which the extraction takes place. For this purpose, we consider here the effect of solid barriers downstream of the dampers on the reduction of the confinement velocity and on the stratification conditions.

The study was carried out in the same conditions as those established in the § 3.2. The results, shown in Fig. 15, are presented in terms of a dimensionless number R_c; defined as the ratio between the confinement velocity in the tunnel with barriers and the confinement velocity in the tunnel with no barriers (for the same conditions). This ratio is written in the form $R_c = \frac{U_{0,c \text{ with barriers}}}{U_{0,c \text{ without barriers}}}$ and the quantity (1 - R_c) characterises the reduction rate of the confinement velocity due to the presence of the barrier. It was verifies that the confinement velocity reduction was the same for both sides of the tunnel. As shown in Fig. 15, the reduction of the confinement velocity is independent of the source conditions (i.e. in all cases the ratio R_c is independent of Γ_i). But it is very different according to the shape of the dampers.

With the rectangular-shaped dampers in place, the effect of the barriers on the reduction of the confinement velocities is very low (the reduction is less than 10% and is almost the same for both barriers $H/4$ and $H/3$). We have to conclude that the

rectangular dampers are so effective in the smoke extraction, that the presence of the barriers has a very little effect on the smoke confinement. In tunnels equipped with such dampers, the use of barriers is therefore not necessary.

With the square-shaped dampers in place, the results show instead that the barriers can significantly reduce the confinement velocities. This reduction increases with the height of the barriers and depends only slightly on the position of the dampers: it is slightly better with dampers placed in the centre of the tunnel ceiling where the reduction rates (1 - R_c) are 38% and 58% (with the barriers H/4 and H/3) against 32% and 55% with dampers placed on the side. This means that, in this case, the barriers can effectively control the spread of smoke downstream of the dampers even for relatively low extraction flow rates. They block the smoke that accumulates close to the dampers and is then easily extracted by the exhaust ducts. The smoke remains completely confined in the area between the two positions of the dampers, unlike the case with no barriers where a small layer of smoke appears downstream of the dampers, particularly with the dampers placed at the edge of the tunnel, even if the extraction rate is very high (as shown in Fig. 14).

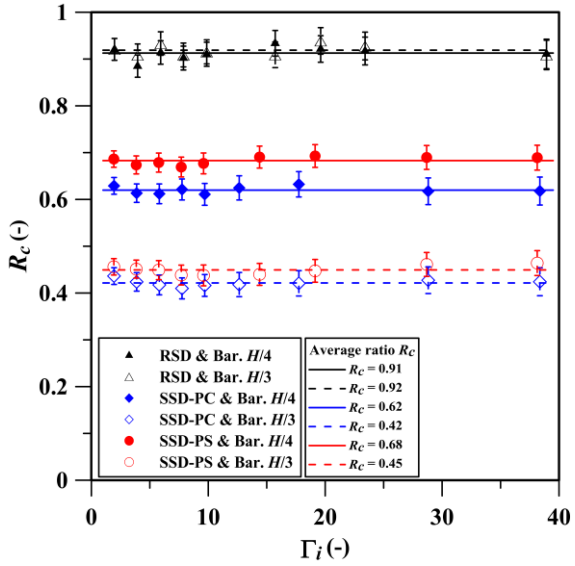

Fig. 15. The velocity ratio R_c -given by the confinement velocity in the tunnel with barriers to the confinement velocity in the empty tunnel- against the plume Richardson number Γ_i, for different shapes and locations of the exhaust vents and with both barriers of height H/4 and H/3.

Fig. 16 shows a typical example of the visualisation of smoke behaviour in the tunnel with and without barriers equipped with square-shaped dampers placed on the side (i.e. case in which the confinement flow rates are higher and the level of stratification is worse). The three flow visualisations are obtained for same source conditions (Γ_i = 40, ρ_i/ρ_0= 0.7 and D_i/H = 0.56) but for different ventilation flow. Fig. 16a shows the configuration with no barriers, which is the same as that presented previously in Fig. 14c, where we have seen that the stratification of the gases is completely disturbed even before reaching the confinement conditions. The visualisation of the flow in the tunnel with a barrier of height h = H/4 is presented in Fig. 16b. In this case, the total confinement is reached for a $Fr_{0,c}$ = 0.75 and the stratification condition of the smoke is better preserved compared to the case of a tunnel without barriers. Small vortices appear and disappear at the interface between the smoke layer and the underlying air flow, but the mixing between the two is small. The behaviour of the confinement smoke can therefore be considered to be in a transition between the stable and unstable stratification regime, which is however significantly different from the unstable regime observed in the case without barriers (Fig. 16a). The visualisation of the smoke flow in the tunnel with the largest barrier (H/3) is presented in Fig. 16c. In this case, the confinement Froude number is reduced by 55% of its reference value, i.e. in the tunnel without barriers. The stratification of the smoke layer is well preserved so that its behaviour can be identified as a 'stable' regime. This means that the barrier H/3 allows a complete confinement of the smoke with a transition from an unstable stratification regime in the empty tunnel (Fig. 16a) to a fully stable regime in the tunnel with largest barriers (Fig. 16c). The presence of these barriers therefore results in

an increased efficiency of the mechanical extraction systems and thus in an improvement of the safety conditions for the tunnel users.

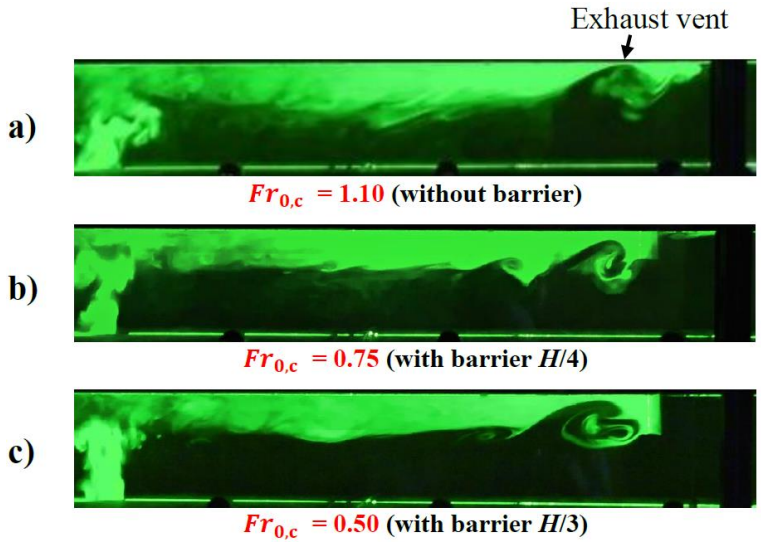

Fig. 16. Visualisation of the smoke flow in the tunnel equipped with square shaped dampers placed on one of the sides of the tunnel ceiling (confinement conditions with Γ_i = 40). a) Tunnel without barriers ($Fr_{0,c}$ = 1.10). b) Tunnel with a large barrier $H/4$ ($Fr_{0,c}$ = 0.75). c) Tunnel with a largest barrier of height $H/3$ ($Fr_{0,c}$ = 0.50).

4 CONCLUSIONS

In this study, we performed a series of experiments in a small-scale tunnel to study the propagation of buoyant smoke injected into a tunnel where the plume is confined between two exhaust vents located on each side of the source. Our analysis focuses on two main geometrical parameters: the shape of the dampers (square and rectangular with same surface area) and the position of the square-shaped dampers (in the centre and on the side of the tunnel ceiling). Our aim was to evaluate the influence of these parameters on i) the backflow length downstream of the dampers, ii) the confinement velocity and iii) the preservation of the stratification of the smoke flow. The main findings are:

- The back-layering length decreases more rapidly with rectangular shaped dampers. Its evolution, in the case of square-shaped dampers, begins with a rapid decline followed by a slight decrease when $L/H \approx 1$.
- The Froude number defined as $Fr_{0,c} = U_{0,c}/(B_i/H)^{1/3}$ $\left(\text{or as } Fr_{0,c} = U_{0,c}/(Q_c/H)^{1/3} \text{ for a fire plume}\right)$ is the only flow control parameter. The confinement conditions are reached with a constant Froude number, this gives the relationship between $U_{0,c}$ and B_i/H (or Q_c/H) as follows: $U_{0,c} = Fr_{0,c}\,(B_i/H)^{1/3}$ $\left(\text{or } U_{0,c} = Fr_{0,c}\,(Q_c/H)^{1/3}\right)$. The proportionality factor ($Fr_{0,c}$) depends on both the shape and the position of the dampers, its values are lowest with the rectangular dampers and are highest with the square dampers placed on the side of the tunnel ceiling.
- The stratification of the smoke layer is affected by the extraction rate. The higher the flow rate, the more unstable the smoke stratification. Depending on the Froude number, the flow configurations can be classified into three regimes: stable, transient and unstable.
- The confinement conditions are achieved in the stable regime with rectangular dampers, in the transition regime with square dampers placed in the centre and in unstable regime with square dampers placed on the side.

In conclusion, the shape and location of the dampers play an important role on the control of smoke in transverse ventilation tunnels. The results highlight two main features: first, the width of the damper is the relevant length scale; the larger it is, the better the smoke control and the second, the location of the vents on the tunnel ceiling is critical; the closer they are to the centre, the more effective they are.

Subsequently, we evaluated the effectiveness of solid barriers, placed at the tunnel ceiling downstream of the dampers, on improving the efficiency of the ventilation system. The results showed that they only have an influence when the width of the dampers are smaller than the width of the tunnel. In such a case, the confinement velocity is significantly reduced and the stratification level of the smoke layer is greatly enhanced, especially when the height of the barrier is large.

These results provide interesting indications for the optimisation of transverse ventilation systems. The reduction of the extraction flow rates is first and foremost an economical solution, since it allows for a reduction of the energy consumption. In addition, the definition of the optimal flow rate is also essential to ensure the safety of the tunnel users, by identifying the ventilation conditions preserving the stratification of the smoke layer confined between the two dampers. Installing mobile barriers can help with this, these barriers improve the performance of the smoke extraction system and therefore ensure a highest level of safety for users in the instance of a fire.

In this study, we focused on geometrical configurations of the dampers in which their distance from the buoyant source was fixed, and equal to 5*H*. Further work will be then needed to study the effect of asymmetric dampers location (relative to the source position), of the variation of the distance between the source and the dampers, of the variation of the cross-sectional area of the extractor vents as well of the presence of traffic flows on the smoke propagation [31] will be studied. Other research work will also have to investigate the role of heat losses induced by radiation and thermal conduction at tunnel walls (see Salizzoni et al. [30] for a similar study in the case of longitudinal ventilation).

ACKNOWLEDGMENTS

This work was supported by the Région Auvergne Rhône-Alpes and in partnership with Centre d'Etude des Tunnels (CETU).

REFERENCES

1 O. Vauquelin, Experimental simulations of fire-induced smoke control in tunnels using an "air–helium reduced scale model": Principle, limitations, results and future, Tunnelling and Underground Space Technology 23, no 2, pp. 171-78, 2008.

2 P. H. Thomas, The movement of smoke in horizontal passages against an air flow, Fire Research Note, No. 723, Fire Research Station, Watford, UK, 1968.

3 N. Danziger, W. Kennedy, Longitudinal ventilation analysis for the Glenwood canyon tunnels, 4th International Symposium Aerodynamics & Ventilation of Vehicle Tunnels, p. 169–186, 1982.

4 Y. Oka, G.T. Atkinson, Control of smoke flow in tunnel fires. Fire Saf. J., 25(4):305–322, 1995.

5 Y. Wu, M. Bakar, Control of smoke flow in tunnel fires using longitudinal ventilation systems - a study of the critical velocity, Fire Saf. J., vol. 35, pp. 363–390, 2000.

6 O. Vauquelin, O. Mégret, Smoke extraction experiments in case of fire in a tunnel, Fire Safety Journal 37, no 5, pp. 525-33, 2002.

7 O. Vauquelin, D. Telle, Definition and experimental evaluation of the smoke "confinement velocity" in tunnel fires, Fire Safety Journal 40, no 4, pp. 320-30, 2005.

8 Y. F. Wang, J. Jiang, D. Zhu, Full-scale experiment research and theoretical study for fires in tunnels with roof openings, Fire Saf. J. 44 (3), pp. 339–348, 2009.

9 Y. F. Wang, T. Qin, X. F. Sun, S. Liu and J. C. Jiang, Full-scale fire experiments and simulation of tunnel with vertical shafts, Appl. Therm. Eng. 105, pp. 243-55, 2016.

10 H. Ingason and Y. Z. Li, Model Scale Tunnel Fire Tests with Point Extraction Ventilation, Journal of Fire Protection Engineering 21, no 1, pp. 5-36, 2011.

11 C. G. Fan, J. Ji, Z. H. Gao, J. Y. Han and J. H. Sun, Experimental study of air entrainment mode with natural ventilation using shafts in road tunnel fires, International Journal of Heat and Mass Transfer 56, no 1, pp. 750-57, 2013.

12 L.J. Li, Z. H. Gao, J. Ji, J.Y. Han and J.H. Sun, Research on the Phenomenon of Plug-holing under Mechanical Smoke Exhaust in Tunnel Fire, Procedia Engineering, 9th Asia-Oceania Symposium on Fire Science and Technology 62, pp. 1112-20, 2013.

13 D. Spratt and A. J. M. Heselden, Efficient extraction of smoke from a thin layer under a ceiling, Fire Research Note No. 1001. U.K. Joint Fire Research Organization, 1974.

14 H. P. Morgan and J. P. Gardiner, Design principles for smoke ventilation in enclosed shopping centers, BR186. Garston, U.K.: Building Research Establishment, 1990.

15 G. D. Lougheed, G. V. Hadjisophocleous, C. McCartney and B. C. Taber, Large-scale Physical Model Studies for an Atrium Smoke Exhaust System, ASHRAE Transactions, v. 105, pt.1, pp. 1-23, 1999.

16 J. Ji, Z. H. Gao, C. G. Fan, W. Zhong and J. H. Sun, A study of the effect of plug-holing and boundary layer separation on natural ventilation with vertical shaft in urban road tunnel fires, Inter. J. of H. and M. Tr. 55, no 21, pp. 6032-6041, 2012.

17 X. Jiang, X. Liao, S. Chen, J. Wang and S. Zhang, An experimental study on plug-holing in tunnel fire with central smoke extraction, Appl. Therm. Eng. 138 pp. 840-848, 2018.

18 L. Yi, R. Wei, J. Peng, T. Ni, Z. Xu and D. Wu, Experimental study on heat exhaust coefficient of transversal smoke extraction system in tunnel under fire, Tunnelling and Underground Space Technology 49, pp. 268-78, 2015.

19 T. Du, D. Yang, S. Peng, Y. Liu and Y. Xiao, Performance evaluation of longitudinal and transverse ventilation for thermal and smoke control in a looped urban traffic link tunnel, Appl. Therm. Eng. 96, pp. 490–500, 2016.

20 L. X. Yu, F. Liu, Y. Q. Liu, M.C. Weng and S. J. Liao, Experimental study on thermal and smoke control using transverse ventilation in a sloping urban traffic link tunnel fire, Tunnelling and Underground Space Technology 71 pp. 81-93, 2018.

21 P. Zhao, Z. Yuan, Y. Yuan, N. Yu and T. Yu, A Study on Ceiling Temperature Distribution and Critical Exhaust Volumetric Flow Rate in a Long-Distance Subway Tunnel Fire with a Two-Point Extraction Ventilation System, Energies 12, no 8, p. 1411, 2019.

22 R. Harish, and K. Venkatasubbaiah, Effects of buoyancy induced roof ventilation systems for smoke removal in tunnel fires, Tunnelling and Underground Space Technology 42, pp. 195-205, 2014.

23 H. H. Zhu, Y. Shen, Z. G. Yan, Q. C. Guo and Q. H. Guo, A numerical study on the feasibility and efficiency of point smoke extraction strategies in large cross-section shield tunnel fires using CFD modeling, Journal of Loss Prevention in the Process Industries 44, pp. 158-170, 2016.

24 Q. Liang, Y. Li, J. Li, H. Xu and K. Li, Numerical studies on the smoke control by water mist screens with transverse ventilation in tunnel fires, Tunnelling and Underground Space Technology 64, pp. 177-83, 2017.

25 E.J. Lee, C.B. Oh, K.C. Oh, Y.H. Yoo and H.J. Shin, Performance of the smoke extraction system for fires in the Busan-Geoje immersed tunnel, Tunn. Undergr. Space Technol., 25 (5), pp. 600-606, 2010.

26 L.F. Chen, L.H. Hu, X.L. Zhang, X.Z. Zhang, X.C. Zhang, L.Z. Yang, Thermal buoyant smoke back-layering flow length in a longitudinal ventilated tunnel with ceiling extraction at difference distance from heat source. Appl. Therm. Eng. 78, 129–135, 2015.

27 Y. Yao, X. Cheng, S. Zhang, K. Zhu, L. Shi, H. Zhang, Smoke back-layering flow length in longitudinal ventilated tunnel fires with vertical shaft in the upstream, Appl. Therm. Eng., vol. 107, pp. 738-746, 2016.

28 F. Tang, L.J. Li, M.S. Dong, Q. Wang, F.Z. Mei, L.H. Hu, Characterization of buoyant flow stratification behaviors by Richardson (Froude) number in a tunnel fire with complex combination of longitudinal ventilation and ceiling extraction. Appl. Therm. Eng. 110, 1021–1028, 2017.

29 L. Jiang, M. Creyssels, P. Salizzoni, R. Perkins, A. Mos, Critical velocity in inclined tunnels, ISAVFT 17, 13-15 September 2017, Lyon, France.

30 P. Salizzoni, M. Creyssels, L. Jiang, A. Mos, R. Mehaddi, O. Vauquelin, Influence of source conditions and heat losses on the upwind back-layering flow in a longitudinally ventilated tunnel, Intl J Heat and Mass Transfer vol. 117, pp. 143–153, 2018.

31 F. Chaabat, M. Creyssels, A. Mos, J. Wingrave, H. Correia, M. Marro and P. Salizzoni, The effects of solid barriers and blocks on the propagation of smoke within longitudinally ventilated tunnels, Building and Environment, vol. 160, August 2019, 106207.

32 L. Jiang, M. Creyssels, A. Mos, P. Salizzoni, Critical velocity in ventilated tunnels in the case of fire plumes and densimetric plumes, Fire Saf. J., vol. 101, pp. 53-62, 2018.

33 O. Mégret, O. Vauquelin, P. Chassé and E. Casalé, A reduced scale tunnel for the study of fire-induced smoke control, Third International Conference on Safety in Road and Rail Tunnels. Nice, France: ITC, 1998.

34 J. Le Clanche , P. Salizzoni, M. Creyssels, R. Mehaddi , F. Candelier, O. Vauquelin, Aerodynamics of buoyant releases within a longitudinally ventilated tunnel, Experimental Thermal and Fluid Science 57, pp. 121–127, 2014.

35 L. Jiang, M. Creyssels, G. R. Hunt and P. Salizzoni, Control of light gas releases in ventilated tunnels, Journal of Fluid Mechanics, vol. 872, pp. 515-531, 2019.

36 B.R. Morton, G.I. Taylor, J.S. Turner, Turbulent gravitational convection from maintained and instantaneous sources, Proc. R. Soc. Lond. A 234, pp. 1–23, 1956.